A Broadband Wide Angle Metamaterial Absorber for Defense Applications

Somak Bhattacharyya, Saptarshi Ghosh, Devkinandan Chaurasiya and Kumar Vaibhav Srivastava
Department of Electrical Engineering, Indian Institute of Technology, Kanpur-208016, India

Abstract — This paper presents an ultra-thin metamaterial absorber with L-shaped patches placed diagonally at the top surface. The geometrical dimensions of the unit cell have been optimized in such a way that the structure shows broadband response in C-band. Furthermore, an absorption bandwidth of 2.6 GHz is realized with more than 90% absorptivity level ranging from 4.6 to 7.2 GHz. The proposed structure has been studied under oblique incidence, both for TE and TM polarizations where it shows wideband absorption upto 45° incident angles in both the cases. The structure is fabricated and the experimental results are in good agreement with the simulated responses.

Index Terms — Metamaterials, Microwave Absorber, Broadband Absorber, Wide Angle Incidence.

I. INTRODUCTION

Recently, metamaterials based absorbers have found potential interest in different frequency ranges for their compactness [1-3]. But, due to the high Q, it was difficult to achieve high bandwidth using these structures [4-6]. A number of structures have been proposed as multiband as well as bandwidth-enhanced applications employing variations of geometrical dimensions of the unit cell [7-11]. Structures comprising of a number of layers with different unit cell structures have also been reported as bandwidth-enhanced applications [12-13]. Recently, lumped circuit elements have also been incorporated at the top surface for bandwidth-enhanced applications [14-15].

In this paper, a single-layer structure behaving as C-band metamaterial absorber has been proposed. The structure consists of an array of unit cells with two simple L-shaped patches placed diagonally. All the geometrical dimensions of the metallic 'L' have been optimized in such a way that the structure exhibits full width half maxima (FWHM) bandwidth covering the entire C-band. Additionally, absorption bandwidth of 2.6 GHz has been achieved with more than 90% absorptivity ranging from 4.6 GHz to 7.2 GHz. The structure has been fabricated and the experimental response is in good agreement with the simulated ones. The proposed structure has been studied theoretically and experimentally under oblique incidences with both TE and TM polarizations revealing that the absorption bandwidth has been maintained upto incident angle of 45°.

II. DESIGN OF THE STRUCTURE

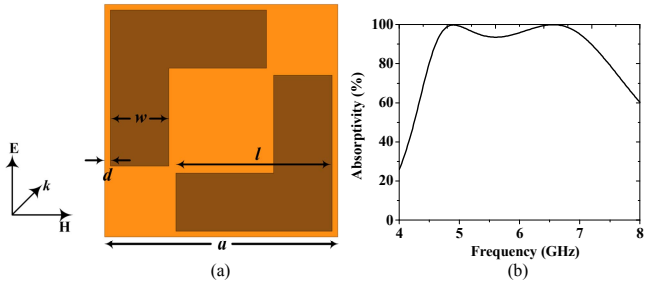

Fig. 1(a) Front view and (b) absorptivity of the proposed broadband absorber (a = 10 mm, w = 2.5 mm, d = 0.25 mm, l = 6.7 mm).

The front view of the proposed structure is shown in Fig. 1(a) where the directions of electric field, magnetic field and incident electromagnetic wave are provided. The metallic L-shaped patches are made up of copper (conductivity of 5.8 x 10^7 S/m). The backside of the structure is completely copper laminated and separated by a single layer of 3.2 mm thick FR-4 substrate (ε_r = 4.05 and $tan\delta$ = 0.02) from its front surface. All the copper films are 0.035 mm thick and other geometrical dimensions are optimized as mentioned in Fig. 1(a) so that broadband absorption occurs across the complete C-band. Due to the complete copper backing, there is no transmission of the incident electromagnetic wave and thus by minimizing the reflection from the structure, the absorption within the structure can be maximized.

III. SIMULATED RESULTS

The proposed L-shaped structure has been simulated using periodic boundary conditions in Ansys HFSS and the FWHM bandwidth covering the complete C-band has been observed. Moreover, absorption bandwidth with more than 90% absorptivity of 2.6 GHz has been observed between 4.6 - 7.2 GHz with peak absorptivities of 99.8% and 99.9% at 4.90 GHz and 6.56 GHz respectively as shown in Fig. 1(b).

The surface currents at the top and bottom metallic surfaces are shown in Fig. 2 and Fig. 3 at the peak absorption frequencies viz., 4.90 GHz and 6.56 GHz. The anti-parallel surface currents at the two metallic patches as evident from Fig. 2 and Fig. 3 form a circular current loop within the substrate, which is controlled by the incident magnetic field, thus creating magnetic excitation. The induced electric fields within the structure are also shown in

978-1-4799-6317-1/14/$31.00 ©2014 IEEE

Fig. 4 at these two frequencies, creating electric excitation. The overlapping of these two excitations results in strong electromagnetic absorption.

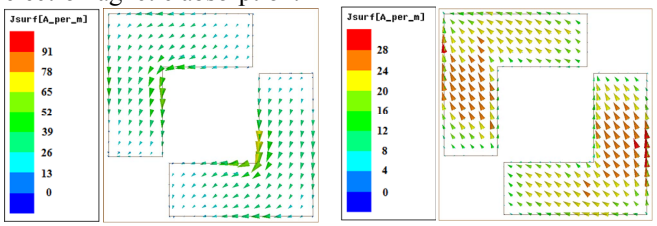

(a) 4.90 GHz (b) 6.56 GHz

Fig. 2. Surface current density distributions at the top surface of the proposed structure.

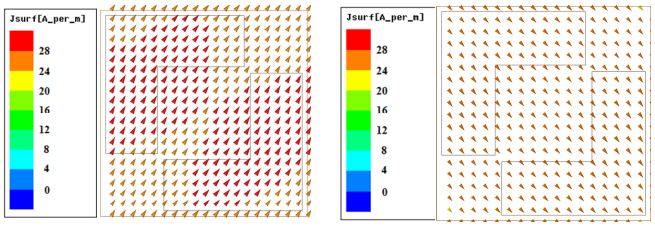

(a) 4.90 GHz (b) 6.56 GHz

Fig. 3. Surface current density distributions at the bottom surface of the proposed structure.

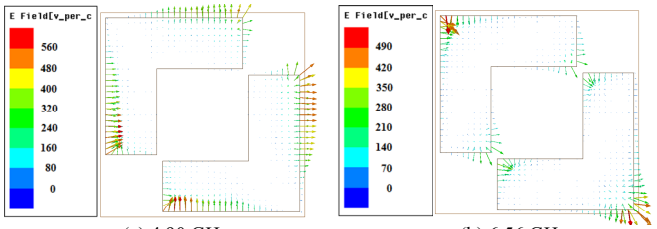

(a) 4.90 GHz (b) 6.56 GHz

Fig. 4. Electric Field distributions within the proposed structure.

The absorptivity responses of the structure are studied under variation of the dimension of the unit cell (a) and patch length (l) as shown in Fig. 5(a) and Fig. 5(b) respectively. As a increases, the gap between adjacent metallic patches increases, reducing the equivalent fringing capacitance. This leads to the increase of the frequency of absorption as evident from Fig. 5(a). With increase of l, the effective inductance increases, leading to the decrease of lowermost frequency of absorption. It is seen from Fig. 4 that along the patch length l, the electric field gets perturbed along the patch at 4.90 GHz, whereas at 6.56 GHz, the electric field will not be much affected as it is primarily concentrated at the corner of the patch. Thus, the upper frequency of absorption will not be changed with variation of l as observed in Fig. 5(b). This leads to increase of bandwidth of absorption with the increase in patch length (l).

The structure is also studied under variation of thickness and real part of permittivity of the dielectric substrate. As thickness (t) increases, the fringing field increases, thereby reducing the frequency of absorption [16]. Also, with the increase of the substrate thickness, more energy will be trapped within the dielectric substrate providing more loss thereby increasing the bandwidth as observed from Fig. 6(a). With the increase of the real part of permittivity (ε_r) of the dielectric substrate (FR-4), the effective capacitance increases, leading to the decrease in frequency of the complete absorption spectrum as evident from Fig. 6(b).

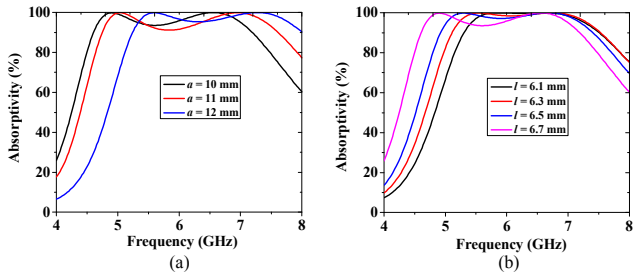

(a) (b)

Fig. 5. Absorptivity variation with respect to variation of (a) unit cell dimension (a) and (b) patch length (l) of the proposed structure.

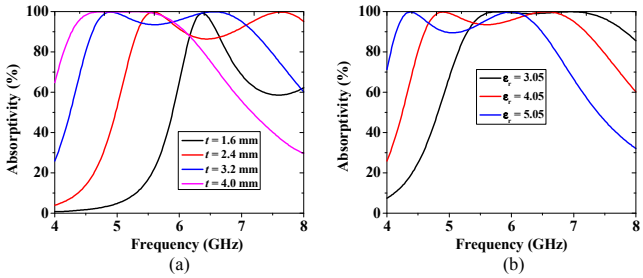

(a) (b)

Fig. 6. Absorptivity response of the structure with respect to variation of (a) thickness (t) and (b) real part of permittivity (ε_r) of the dielectric substrate.

IV. Experimental Results

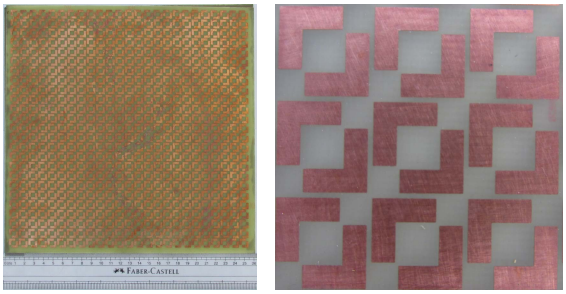

(a) (b)

Fig. 7(a) Top view of the fabricated metamaterial absorber structure with (b) enlarged view.

The proposed structure has been fabricated with dimension of 250 mm x 250 mm x 3.2 mm as shown in Fig. 7(a). During the fabrication procedure, the array of L-shaped pattern is printed on the top side of a 1.6 mm thick FR-4 substrate where the bottom side is completely etched up. Another identical FR-4 substrate of 1.6 mm thickness is completely etched up on one side, maintaining full copper lamination on the other side. These two FR-4 layers are glued together while the etched surfaces are placed back-to-

back. The top view of the fabricated structure is shown in Fig. 7(a) whose enlarged portion is shown in Fig. 7(b).

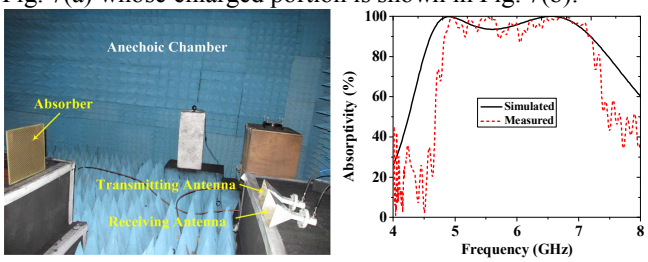

(a) (b)

Fig. 8(a) Experimental arrangement within the anechoic chamber along with (b) comparison between the simulated and measured absorptivity responses.

Initially, a copper sheet with identical dimension to that of the fabricated structure is kept within anechoic chamber and the power reflected from the copper surface is measured and taken as reference. Then, power reflected from the front surface of the fabricated structure is measured. The difference between the reflected powers provides exact reflected power from the fabricated structure which gives rise to the measure of absorptivity. A pair of identical C-band horn antennas (J-5041) and Vector Network Analyzer (VNA) Agilent N5320A are used to measure reflected power. One of these antennas is used to transmit electromagnetic wave while the other one is used to receive the power reflected from the structure. The complete experimental setup incorporating the fabricated structure and the pair of antennas within the anechoic chamber is shown in Fig. 8(a). The measured absorptivity response is shown in

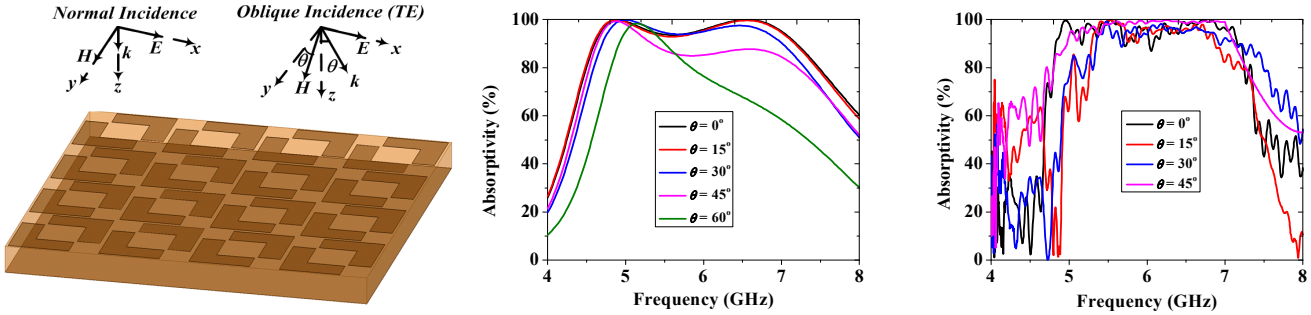

(a) (b) (c)

Fig. 9(a) Set up for the oblique incidence response under TE polarization with (b) simulated and (c) measured absorptivity responses.

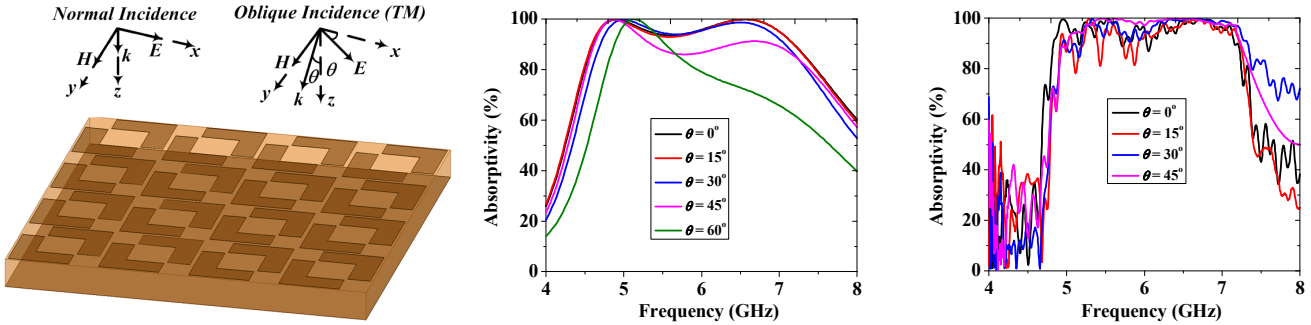

(a) (b) (c)

Fig. 10(a) Set up for the oblique incidence response under TM polarization with (b) simulated and (c) measured absorptivity responses.

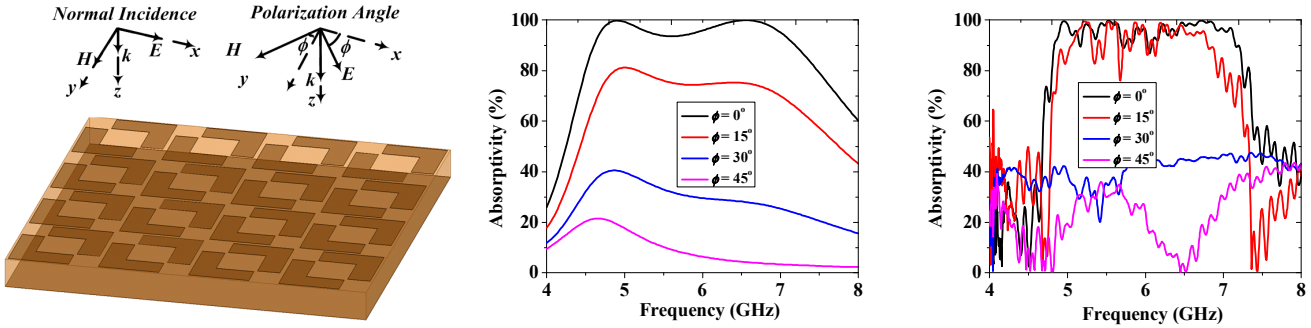

(a) (b) (c)

Fig. 11(a) Set up for the structure under polarization angle variation with (b) simulated and (c) measured absorptivity responses.

Fig. 8(b), where it is compared with the simulated response. The FWHM bandwidth of 3.2 GHz ranging from 4.6 GHz to 7.8 GHz has been measured. Also, absorption bandwidth of 2.33 GHz with more than 90% absorptivity ranging from 4.82 GHz to 7.15 GHz has been experimentally achieved. The absorption peaks are found at 4.95 GHz and 6.57 GHz with peak absorptivities of 98.9% and 99.1% respectively, which are slightly different from the simulated absorption peaks due to fabrication tolerances.

V. Responses under Oblique Incidence and Polarization Angle Variations

A. Variation of the Incident Angle

The structure is simulated for different angles of incidence (θ) as shown in Fig. 9(a), under TE polarization. In this case, the electric field is retained towards *x*-direction, while the directions of magnetic field and wave vector are changed by an angle θ. The simulated and the measured absorptivity responses are shown in Fig. 9(b) and Fig. 9(c) respectively. The wide absorption bandwidth is maintained upto 45° incident angle in both cases.

The structure is also studied for different incident angles under TM polarization as illustrated in Fig. 10(a). Here, the magnetic field is oriented along *y*-direction, while the directions of electric field and wave vector are varied by an angle θ. The simulated and the measured absorptivity responses are given in Fig. 10(b) and Fig. 10(c) respectively. Upto 45° incident angle, the wide absorption bandwidth is observed both theoretically and experimentally.

B. Variation of the Polarization Angle

The proposed structure has also been studied for different angles of polarization (ϕ) as shown in Fig. 11(a), where the wave propagation direction remains parallel to *z*-direction while both the electric and magnetic field make an angle ϕ with *x*-direction and *y*-direction respectively. Due to the two-fold symmetry of the structure along *xy* plane, the structure is studied only upto 45° angle of polarization. The simulated absorptivity response is shown in Fig. 11(b), revealing that the structure exhibits broadband absorption upto 15° polarization angle. The experimental response shown in Fig. 11(c) is also in good agreement with the simulated one.

VI. Conclusions

A complete C-band metamaterial absorber has been discussed with two simple L-shaped patches made up of copper placed diagonally at the top surfaces. The proposed structure shows 2.6 GHz absorption bandwidth with more than 90% absorptivity in the C-band. The structure is only 3.2 mm thick ($\sim \lambda/15$ with respect to the center frequency). The roles of several geometrical parameters of the structure have been studied to explain the broadband nature of the absorber. The structure is fabricated and the broadband absorptivity response is achieved experimentally too. The proposed structure exhibits wide absorption bandwidth upto 45° incident angles for TE and TM polarizations as evident from simulated and experimentally measured responses. The proposed structure can be applied for the commercial air defense applications.

References

[1] M.H.Li, L.Hua Yang, B.Zhou, X.Peng Shen, Q.Cheng, and T.J.Cui, "Ultrathin multiband gigahertz metamaterial absorbers," *Journal of Applied Physics*, Vol. 110, Issue 1, pp. 014909, 2011.

[2] H.Tao, N.Landy, C.M.Bingham, X.Zhang, R.D.Averit, and W.J.Padilla, "A metamaterial absorber for the terahertz regime: design, fabrication and characterization," *Optics Express*, Vol. 16, No. 10, pp. 7181-7188,May 2008.

[3] N.Zhang, P.Zhou, D.Cheng, X.Weng, J.Xie, and L.Deng, "Dual-band absorption of mid-infrared metamaterial absorber based on distinct dielectric spacer layers," *Optics Letters*, Vol. 38, No. 7, pp. 1125-1127, 1 April, 2013.

[4] S.Bhattacharyya, H.Baradiya, and K.V.Srivastava, "An Ultra Thin Metamaterial Absorber using Electric Field Driven LC Resonator with Meander Lines," *2012 IEEE International Symposium on Antennas and Propagation and USNC/URSI National Radio Science Meeting*, pp. 1-2, July, 2012.

[5] S.Bhattacharyya, S.Ghosh, H.Baradiya, and K.V.Srivastava, "Study on Ultra-thin Dual Frequency Metamaterial absorber with Retrieval of Electromagnetic Parameters," *2014 Twentieth National Conference on Communication,* pp. 1-6, 28 February-2 March, 2014.

[6] S.Bhattacharyya, and K.V.Srivastava, "An Ultra Thin Electric Field Driven LC Resonator Structure as Metamaterial Absorbers for Dual Band Applications," *2013 URSI International Symposium on Electromagnetic Theory (EMTS)*, pp. 722-725, 2013.

[7] S.Bhattacharyya, S.Ghosh, and K.V.Srivastava, "Bandwidth enhanced metamaterial absorber using electric field driven LC Resonator for airborne radar applications," *Microwave and Optical Technology Letters*, Vol. 55, Issue 9, pp. 2131-2137, September 2013.

[8] S.Ghosh, S.Bhattacharyya, and K.V.Srivastava, "Bandwidth-enhancement of an ultra-thin polarization insensitive metamaterial absorber," *Microwave and Optical Technology Letters*, Vol. 56, Issue 2, pp. 350-355, February 2014.

[9] S.Bhattacharyya, and K.V.Srivastava, "Triple band polarization-independent ultra-thin metamaterial absorber using ELC resonator," *Journal of Applied Physics*, Vol. 115, Issue 6, pp. 064508, 2014.

[10] S.Bhattacharyya, S.Ghosh, and K.V.Srivastava, "Triple band polarization-independent metamaterial absorber with bandwidth enhancement at X-band," *Journal of Applied Physics*, Vol. 114, Issue 9, pp. 094514, 2013.

[11] S.Ghosh, S.Bhattacharyya, Y.Kaiprath, and K.V.Srivastava, "Bandwidth-enhanced Polarization Insensitive Microwave Metamaterial Absorber and its Equivalent Circuit Model," *Journal of Applied Physics*, Vol. 115, Issue 10, pp. 104503, 2014.

[12] J.Sun, L.Liu, G.Dong, and L.Zhou, "An extremely broadband metamaterial absorber based on destructive interference," *Optics Express*, Vol. 19, Issue 22, 24 October 2011, pp. 21155-21162.

[13] H.Xiong, J.S.-Hong, C.M.-Luo, and L.-L.Hong, "An ultrathin and broadband metamaterial absorber using multi-layer structures," *Journal of Applied Physics*, Vol. 114, Issue 6, 2013, pp. 064109.

[14] S.Li, J.Guo, X.Cao, W.Li, Z.Zhang, and D.Zhang, "Wideband, thin, and polarization-insesnsitive perfect absorber based on the double octagonal rings metamaterials and lumped resistances," *Journal of Applied Physics*, Vol. 116, Issue 4, 2014, pp. 043710.

[15] W.Yuan, and Y.Cheng, "Low-frequency and broadband metamaterial absorber based on lumped elements: design, characerization and experiment," *Applied Physics A*, *Materials Science & Processing*, 31 July 2014, pp. 1-7.